

Spin anisotropic interactions of lower-polaritons in the vicinity of polaritonic Feshbach resonance

N. Takemura,^{1,*} M. D. Anderson,¹ M. Navadeh-Toupchi,¹ D. Y. Oberli,¹ M. T. Portella-Oberli,¹ and B. Deveaud¹

¹*Laboratory of Quantum Optoelectronics, Institute of Physics,
École Polytechnique Fédérale de Lausanne, CH-1015, Lausanne, Switzerland*

(Dated: December 3, 2024)

We determine experimentally the spinor interaction constants of lower-polaritons α_1 and α_2 using resonant pump-probe spectroscopy with a spectrally narrow pump pulse. Our experimental findings are analyzed with the Bogoliubov-like theory and mean-field two channel model based on the lower-polariton and biexciton basis. We find an enhancement of the attractive interaction and dissipative nonlinearity of lower-polaritons with anti-parallel spins in the vicinity of the biexciton resonance when the energy of two lower-polaritons approaches energetically that of the biexciton. These observations are consistent with the existence of a scattering resonance between lower-polaritons and biexcitons (polaritonic Feshbach resonance).

PACS numbers: 78.20.Ls, 42.65.-k, 76.50.+g

I. INTRODUCTION

In semiconductor microcavities, the strong coupling between quantum well excitons and cavity photons gives rise to new eigenstates: lower and upper-polariton.¹ In the last two decades, exciton-polaritons have drawn a large attention of physicists in various fields both in terms of fundamental physics and potential device applications. Among them, recent great achievements are realization of Bose-Einstein condensation² and polariton superfluidity³⁻⁶. In these physics, the non-linearity originating from exciton-exciton interaction plays a central role. Moreover, a spin anisotropy of the exciton interactions emerges from the optically coupled two spin projections of a heavy-hole exciton: $|J_z = \pm 1\rangle = |J_e = \mp 1/2, J_h = \pm 3/2\rangle$. In particular, interactions between excitons with anti-parallel spins allows the formation of a molecular bound state of two excitons, called the biexciton⁷. In cold atom physics, it is well known that the molecular bound state dramatically modifies the interatomic interaction when the energy of incident atoms in an open channel is tuned to that of a molecular state in a closed channel. This is a manifestation of a scattering resonance called Feshbach resonance⁸. Actually, the biexciton also affects the interaction of polaritons when the lower-polariton energy is in the vicinity of the biexciton energy^{9,10}. Experimentally, the signature is an enhancement of the interaction and a large polariton decay associated with a biexciton channel¹¹⁻¹³. These observations can be understood as a polaritonic analogue of the Feshbach resonance: “polaritonic Feshbach resonance”¹². For device applications of semiconductor microcavities, the enhancement of the non-linearity might be useful for non-classical photon generation^{10,14}. Additionally, the polaritonic Feshbach resonance is also interesting in terms of some questions of fundamental physics including a collective paring¹⁵ and formation of bose polarons¹⁶. Moreover, the spin anisotropic polariton interaction is important in regard to the stability of polariton condensates.

For instance, a thermodynamical argument predicts the collapse of polariton condensates when the polariton interaction with anti-parallel spins is stronger than that with parallel spins^{11,17}.

This paper explores the spinor interactions of the two lower-polariton in the vicinity of the polaritonic Feshbach resonance. Experimentally, we employ a polarization selective pump-probe spectroscopy with a spectrally narrow pump pulse. Depending on the polarization configuration of the two pulses (co- and counter-circularly), we can independently access the polariton interaction with parallel (α_1) and anti-parallel spins (α_2). The central idea of the spectroscopic technique that we are using is similar to that of our previous paper¹⁸, except for the fact that the lower- and upper-polariton branches were excited simultaneously with a spectrally broad pump pulse. On the other hand, in this paper, the pump pulse is a spectrally narrow pulse and excites only the lower-polariton branch. This allows the use of the lower-polariton basis in the theoretical model, which dramatically simplifies the analysis by removing complicated effects associated with the upper-polariton branch such as an excitation induced dephasing (EID)¹⁹. We discuss the quasi-stationary behavior of the spinor polariton physics within the Bogoliubov theory and a mean-field two-channel model.

This paper is organized as following. Section II describes the experimental configuration. Section III presents the theoretical background used in our paper. In Section IV, we discuss the experimental results and analyze them. We present conclusions in the last section.

II. EXPERIMENT

The measurements are performed with a high quality III-V GaAs-based microcavity²⁰ at the cryogenic temperature of 4K. A single 8 nm $\text{In}_{0.04}\text{Ga}_{0.96}\text{As}$ quantum well

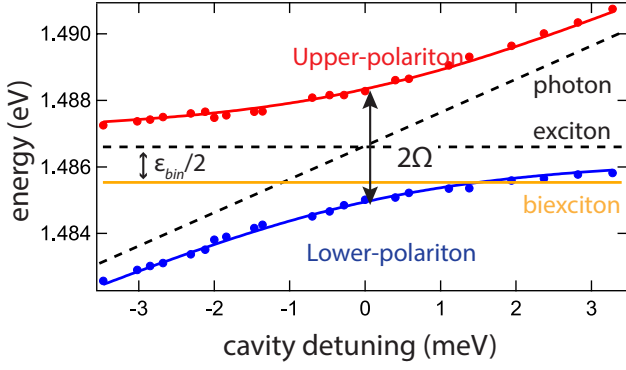


FIG. 1. The energies of the lower and upper-polaritons as a function of the cavity detuning δ at zero in-plane momentum. The energy splitting between the two branches at zero cavity detuning is $2\Omega = 3.45$ meV. The orange line represents the energy of the biexciton represented as $\varepsilon_x - \varepsilon_{bin}/2$, where ε_{bin} is the binding energy of biexcitons

is embedded between a pair of GaAs/AlAs distributed Bragg-reflectors (DBR). The Rabi splitting energy is $2\Omega = 3.45$ meV at zero cavity detuning⁵. Due to the wedge of the cavity spacer, we can adjust the cavity detuning by moving the laser spot over the surface of the sample. Here, the cavity detuning is defined as $\delta = \varepsilon_c - \varepsilon_x$, where ε_c and ε_x are respectively the energies of the uncoupled photon and exciton modes at $\mathbf{k} = 0$. Depending on the cavity detuning, the energy of the lower-polariton varies following the equation:

$$\varepsilon_L = \frac{1}{2}(\varepsilon_c + \varepsilon_x) - \frac{1}{2}\sqrt{(\varepsilon_c - \varepsilon_x)^2 + (2\Omega)^2} \quad (1)$$

The change of the energy of the lower and upper-polaritons is shown in Fig. 1 as a function of the cavity detuning. Figure. 1 shows that by sweeping the cavity detuning, the energy of the two lower-polaritons can cross the biexciton energy.

The sample is excited with a strong pump pulse and probed with a weak probe pulse. Both pump and probe pulses are obtained from a broadband few hundreds femtosecond Ti:Sapphire laser (the linewidth is around 15 meV). After this separation, only the pump pulse is spectrally narrowed with a pulse shaper. The line width of the pump pulse is less than 1 meV. The pump pulse is tuned to the lower polariton energy and then only excites the lower-polariton branch. The in-plane momentum of the pump pulse is $\mathbf{k} = 0 \mu\text{m}^{-1}$. On the other hand, the probe pulse probes both lower- and upper-polariton branches. The center of the probe spectrum is set between the two branches with an in-plane momentum $\mathbf{k} \sim 0 \mu\text{m}^{-1}$. Polarizations of the two pulses are either σ^+ or σ^- . Co- and counter-circular polarization pump-probe configurations produce polaritons with parallel and anti-parallel spins, respectively. The measurements are performed in a transmission configuration. For the detection of the probe pulse, we employ a heterodyne detection technique, which largely suppresses incoherent stray lights

and greatly increases the signal to noise ratio¹⁸. Additionally, we removed the noise originating from the laser spectrum envelope with a numerical low-pass filter. For all experiments, the pump and probe photon densities are respectively fixed as 15×10^{12} photons/pulse/cm² (1 mW) and 3.7×10^{12} photons/pulse/cm² (250 μW). Since the probe pulse is spectrally much broader than the pump, the density produced by the probe pulse is indeed much weaker than by the pump pulse within a single polariton branch. In the main text, all pump-probe measurements are performed at zero pump-probe delay. The pump-probe time delay dependent spectra are discussed in Appendix A.

III. SPINOR GROSS-PITAEVSKII EQUATIONS

In this section, starting from a exciton-photon basis Hamiltonian, we introduce a lower-polariton basis Hamiltonian^{9,21,22} and derive the lower-polariton spinor Gross-Pitaevskii equations. The lower-polariton spinor Gross-Pitaevskii equations is then used as a basis of analysis of the pump-probe spectroscopy.

A. Exciton-photon Hamiltonian

The Hamiltonian written in exciton, photon, and biexciton basis reads:

$$\hat{H} = \hat{H}_{\text{lin}} + \hat{H}_{\text{int}} + \hat{H}_{\text{qm}}. \quad (2)$$

This Hamiltonian is composed of a linear part:

$$\begin{aligned} \hat{H}_{\text{lin}} = & \sum_{\sigma=\{\uparrow\downarrow\}} \int d\mathbf{x} \left[\hat{\psi}_{x,\sigma}^\dagger \left(\varepsilon_x - \frac{\hbar^2 \nabla^2}{2m_x} \right) \hat{\psi}_{x,\sigma} \right. \\ & + \hat{\psi}_{c,\sigma}^\dagger \left(\varepsilon_c - \frac{\hbar^2 \nabla^2}{2m_c} \right) \hat{\psi}_{c,\sigma} \\ & + \hat{\psi}_B^\dagger \left(\varepsilon_B - \frac{\hbar^2 \nabla^2}{2m_B} \right) \hat{\psi}_B \\ & \left. + \Omega (\hat{\psi}_{c,\sigma}^\dagger \hat{\psi}_{x,\sigma} + \hat{\psi}_{x,\sigma}^\dagger \hat{\psi}_{c,\sigma}) \right], \quad (3) \end{aligned}$$

an interacting part:

$$\begin{aligned} \hat{H}_{\text{int}} = & \sum_{\sigma=\{\uparrow\downarrow\}} \int d\mathbf{x} \left[\frac{1}{2} g \hat{\psi}_{x,\sigma}^\dagger \hat{\psi}_{x,\sigma}^\dagger \hat{\psi}_{x,\sigma} \hat{\psi}_{x,\sigma} \right. \\ & + \frac{1}{2} g^{+-} \hat{\psi}_{x,\sigma}^\dagger \hat{\psi}_{x,-\sigma}^\dagger \hat{\psi}_{x,-\sigma} \hat{\psi}_{x,\sigma} \\ & + \frac{1}{2} g_{bx} (\hat{\psi}_B \hat{\psi}_{x,\sigma}^\dagger \hat{\psi}_{x,-\sigma}^\dagger + \hat{\psi}_{x,\sigma} \hat{\psi}_{x,-\sigma} \hat{\psi}_B^\dagger) \\ & \left. - g_{\text{pae}} (\hat{\psi}_{c,\sigma}^\dagger \hat{\psi}_{x,\sigma}^\dagger \hat{\psi}_{x,\sigma} \hat{\psi}_{x,\sigma} + \hat{\psi}_{x,\sigma}^\dagger \hat{\psi}_{x,\sigma}^\dagger \hat{\psi}_{x,\sigma} \hat{\psi}_{c,\sigma}) \right], \quad (4) \end{aligned}$$

and a quasi-mode coupling to the electric field outside the cavity:

$$\hat{H}_{\text{qm}} = \sum_{\sigma=\{\uparrow\downarrow\}} \int d\mathbf{x} \Omega_{qm} (\hat{\psi}_{c,\sigma}^\dagger \mathbf{F}_\sigma + \mathbf{F}_\sigma^* \hat{\psi}_{c,\sigma}). \quad (5)$$

Here, Ω is the Rabi coupling between excitons and photons. \mathbf{F}_σ represents the electric field outside the cavity, while Ω_{qm} is the strength of the quasi-mode coupling. The operator $\hat{\psi}_{x(c),\sigma}$ is a bosonic exciton (photon) operator including spins (circular polarization σ^\pm). The masses of excitons, photons, and biexcitons are respectively expressed as m_x , m_c , and m_B . The energies ε_x , ε_c , and ε_B are respectively the energies of exciton, photon and biexciton with zero momentum. The spin-dependent exciton operators satisfy the following commutation relations:

$$[\hat{\psi}_{x(c),\sigma}(\mathbf{x}), \hat{\psi}_{x(c),\sigma'}^\dagger(\mathbf{x}')] = \delta_{\sigma,\sigma'} \delta(\mathbf{x} - \mathbf{x}') \quad (6)$$

and

$$[\hat{\psi}_{x(c),\sigma}^{(\dagger)}(\mathbf{x}), \hat{\psi}_{x(c),\sigma'}^{(\dagger)}(\mathbf{x}')] = 0. \quad (7)$$

The bosonic biexciton operator $\hat{\psi}_B$ satisfies:

$$[\hat{\psi}_B(\mathbf{x}), \hat{\psi}_B^\dagger(\mathbf{x}')] = \delta(\mathbf{x} - \mathbf{x}') \quad (8)$$

and

$$[\hat{\psi}_B^{(\dagger)}(\mathbf{x}), \hat{\psi}_B^{(\dagger)}(\mathbf{x}')] = 0. \quad (9)$$

In this Hamiltonian, the constants g and g^{+-} respectively represent the effective contact-type exciton-exciton interaction with parallel and anti-parallel spins. We would like to stress the difference between bare non-contact exciton-exciton interaction and an effective contact interaction employed here²³. The term g_{+-} does not exist within the Born approximation, but appears only when higher-order scattering contributions are included. Actually, we will find that this ‘‘background interaction’’ g_{+-} is important to explain our experimental observations. In Appendix B, we discuss how the effective interactions are related to the bare non-contact exciton-exciton interactions. g_{bx} is the exciton-biexciton coupling strength. Finally, the term g_{pae} is a photon assisted exchange scattering²⁴, which originates from the fermionic constituents of an exciton. This interaction is also often referred to as an anharmonic saturation term or ‘‘phase-space filling’’²⁵.

B. Lower polariton Hamiltonian

Now, we introduce the polariton basis $\hat{\psi}_{L(U)}$ defined as

$$\begin{pmatrix} \hat{\psi}_x(\mathbf{x}) \\ \hat{\psi}_c(\mathbf{x}) \end{pmatrix} = \begin{pmatrix} X_0 & -C_0 \\ C_0 & X_0 \end{pmatrix} \begin{pmatrix} \hat{\psi}_L(\mathbf{x}) \\ \hat{\psi}_U(\mathbf{x}) \end{pmatrix}, \quad (10)$$

the Hamiltonian is rewritten with the polariton basis. The coefficients X_0 and C_0 are the Hopfield coefficients at $\mathbf{k} = 0$. They are respectively written as

$$X_0 = \sqrt{\frac{1}{2} \left(1 + \frac{(\varepsilon_c - \varepsilon_x)}{\sqrt{(\varepsilon_c - \varepsilon_x)^2 + (2\Omega)^2}} \right)} \quad (11)$$

and

$$C_0 = -\sqrt{\frac{1}{2} \left(1 - \frac{(\varepsilon_c - \varepsilon_x)}{\sqrt{(\varepsilon_c - \varepsilon_x)^2 + (2\Omega)^2}} \right)}. \quad (12)$$

The field operators of the polariton also satisfy the bosonic commutation relations:

$$[\hat{\psi}_{L(U),\sigma}(\mathbf{x}), \hat{\psi}_{L(U),\sigma'}^\dagger(\mathbf{x}')] = \delta_{\sigma,\sigma'} \delta(\mathbf{x} - \mathbf{x}') \quad (13)$$

and

$$[\hat{\psi}_{L(U),\sigma}^{(\dagger)}(\mathbf{x}), \hat{\psi}_{L(U),\sigma'}^{(\dagger)}(\mathbf{x}')] = 0. \quad (14)$$

Since the pump excites only the lower polariton, we neglect the terms involving the upper polariton operators. Using only the lower-polariton and biexciton operators, the Hamiltonian Eq. 2 is approximated as

$$\hat{H} \simeq \hat{H}_{\text{lin,LP}} + \hat{H}_{\text{int,LP}} + \hat{H}_{\text{qm,LP}}, \quad (15)$$

where $\hat{H}_{\text{lin,LP}}$, $\hat{H}_{\text{int,LP}}$, and $\hat{H}_{\text{qm,LP}}$ are respectively

$$\begin{aligned} \hat{H}_{\text{lin,LP}} = \sum_{\sigma=\{\uparrow\downarrow\}} \int d\mathbf{x} & \left[\hat{\psi}_{L,\sigma}^\dagger (\varepsilon_L - \frac{\hbar^2 \nabla^2}{2m_L}) \hat{\psi}_{L,\sigma} \right. \\ & \left. + \hat{\psi}_B^\dagger (\varepsilon_B - \frac{\hbar^2 \nabla^2}{2m_B}) \hat{\psi}_B \right], \end{aligned} \quad (16)$$

$$\begin{aligned} \hat{H}_{\text{int,LP}} = \sum_{\sigma=\{\uparrow\downarrow\}} \int d\mathbf{x} & \left[\frac{1}{2} \alpha_1 \hat{\psi}_{L,\sigma}^\dagger \hat{\psi}_{L,\sigma}^\dagger \hat{\psi}_{L,\sigma} \hat{\psi}_{L,\sigma} \right. \\ & + \frac{1}{2} g_L^{+-} \hat{\psi}_{L,\sigma}^\dagger \hat{\psi}_{L,-\sigma}^\dagger \hat{\psi}_{L,-\sigma} \hat{\psi}_{L,\sigma} \\ & \left. + \frac{1}{2} g_L^{bx} (\hat{\psi}_B \hat{\psi}_{L,\sigma}^\dagger \hat{\psi}_{L,-\sigma}^\dagger + \hat{\psi}_{L,\sigma} \hat{\psi}_{L,-\sigma} \hat{\psi}_B^\dagger) \right], \end{aligned} \quad (17)$$

and

$$\hat{H}_{\text{qm,LP}} = \sum_{\sigma=\{\uparrow\downarrow\}} \int d\mathbf{x} \Omega_{L,0} (\hat{\psi}_{L,\sigma}^\dagger \mathbf{F}_\sigma + \mathbf{F}_\sigma^* \hat{\psi}_{L,\sigma}). \quad (18)$$

Here, the energy ε_L is given by Eq. 1. The effective polariton mass m_L is obtained as $1/m_L = |X_0|^2/m_x + |C_0|^2/m_c$. The interaction constants α_1 , g_L^{+-} , and g_L^{bx} are respectively defined as

$$\alpha_1 = g X_0^4 + 4g_{pae} X_0^3 |C_0|, \quad (19)$$

$$g_L^{+-} = g^{+-} X_0^4, \quad (20)$$

and

$$g_L^{bx} = g_{bx} X_0^2. \quad (21)$$

The quasi-mode coupling in the polariton basis is expressed as

$$\Omega_{L,0} = \Omega_{qm} C_0. \quad (22)$$

This Hamiltonian is same as the one of the two-channel model in atomic Bose-Einstein condensates, which describes the Feshbach resonance^{26,27}.

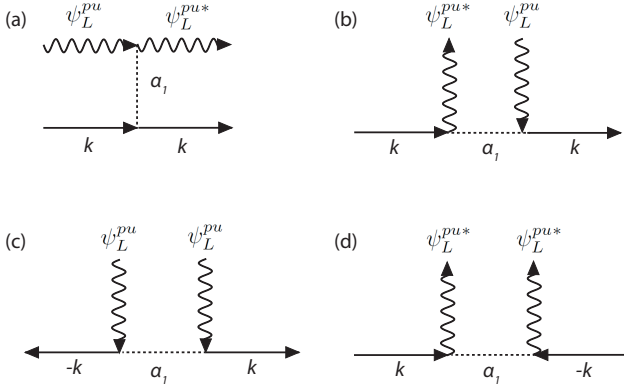


FIG. 2. Diagrammatic representation of polariton interaction with parallel spins. Solid lines represent probe polaritons with momentum \mathbf{k} (right arrow) and $-\mathbf{k}$ (left arrow). The wavy lines represent condensates of the lower polaritons with zero momentum, which is driven by the strong pump beam. The dashed line represents the polariton-polariton interaction with parallel spins α_1 . (a) Hartree-like (direct) process. (b) Fock-like (exchange) process. (c,d) The processes involving the mixing between \mathbf{k} and $-\mathbf{k}$ lower polaritons (Four-wave mixing).

C. Spinor Gross-Pitaevskii of lower polariton and biexciton

We derive the equations of motion of the wavefunctions of lower-polaritons and of biexcitons from the Hamiltonian written in Eq. 15. Combined with a mean-field approximation and an inclusion of phenomenological decay rates of lower-polariton γ_L and biexciton γ_B , the Heisenberg equations of motion lead to coupled equations:

$$i\hbar\dot{\psi}_{L,\uparrow}(\mathbf{x}, t) = \left[\varepsilon_L - i\gamma_L - \frac{\hbar^2\nabla^2}{2m_L} + \alpha_1|\psi_{L,\uparrow}(\mathbf{x}, t)|^2 + g_L^{+-}|\psi_{L,\downarrow}(\mathbf{x}, t)|^2 \right] \psi_{L,\uparrow}(\mathbf{x}, t) + g_L^{bx}\psi_B(\mathbf{x}, t)\psi_{L,\downarrow}^*(\mathbf{x}, t) + f_{ext,\uparrow}(\mathbf{x}, t) \quad (23)$$

and

$$i\hbar\dot{\psi}_B(\mathbf{x}, t) = \left[\varepsilon_B - i\gamma_B - \frac{\hbar^2\nabla^2}{2m_B} \right] \psi_B(\mathbf{x}, t) + g_L^{bx}\psi_{L,\uparrow}(\mathbf{x}, t)\psi_{L,\downarrow}(\mathbf{x}, t), \quad (24)$$

$$\begin{pmatrix} \tilde{\epsilon} - (\varepsilon_L - \varepsilon_{pu} + \frac{\hbar^2\mathbf{k}^2}{2m_L} + 2\alpha_1|\psi_L^{pu}|^2) + i\gamma_L & -\alpha_1\psi_L^{pu2} \\ \alpha_1\psi_L^{pu*2} & \tilde{\epsilon} + (\varepsilon_L - \varepsilon_{pu} + \frac{\hbar^2\mathbf{k}^2}{2m_L} + 2\alpha_1|\psi_L^{pu}|^2) - i\gamma_L \end{pmatrix} \begin{pmatrix} u(\tilde{\epsilon}) \\ v(\tilde{\epsilon}) \end{pmatrix} = \begin{pmatrix} |F^{pr}| \\ 0 \end{pmatrix} \quad (28)$$

The factor two of the $2\alpha_1|\psi_L^{pu}|^2$ in the diagonal element of the matrix is due to the Hartree-like (direct) and

where the driving term $f_{ext,\sigma}$ is defined as $f_{ext,\sigma}(\mathbf{x}, t) = \Omega_{L,0}F_\sigma(\mathbf{x}, t)$. The mean fields of the lower-polariton and biexciton are respectively represented as $\psi_{L,\sigma} = \langle \hat{\psi}_{L,\sigma} \rangle$ and $\psi_B = \langle \hat{\psi}_B \rangle$. We note that the above set of equations is similar to those which describes real time evolutions of the Feshbach molecule in atomic Bose-Einstein condensates²⁶⁻²⁸.

IV. EXPERIMENTAL RESULTS AND ANALYSIS

A. Pump-probe spectroscopy with co-circularly polarized light

Let us first consider the case where the pump and the probe beams are co-circularly polarized. In this configuration, the biexciton cannot be generated, thus, we omit the spin index terms and assume that the biexciton probability amplitude is zero. Now, the equations of motion Eq. 23 and 24 are reduced to the conventional non-equilibrium Gross-Pitaevskii equation for polaritons²⁹:

$$i\hbar\dot{\psi}_L(\mathbf{x}, t) = \left[\varepsilon_L - i\gamma_L - \frac{\hbar^2\nabla^2}{2m_L} + \alpha_1|\psi_L(\mathbf{x}, t)|^2 \right] \psi_L(\mathbf{x}, t) + f_{ext}(\mathbf{x}, t). \quad (25)$$

Now, we try to derive a probe spectrum of interacting polaritons driven by a continuous-wave (CW) pump. First, we assume that a “condensate” exists at $\mathbf{k}_{pump} = \mathbf{0}$ which is driven by the strong pump beam. Secondly we treat the probe beam with a finite momentum \mathbf{k} as a small perturbation:

$$f_{ext}^{pr}(\mathbf{x}, t) = |F^{pr}| e^{-i(\tilde{\epsilon} + \varepsilon_{pu})t/\hbar} e^{i\mathbf{k}\mathbf{x}}. \quad (26)$$

Due to the existence of the “condensate”, we can apply the well-known Bogoliubov theory for weakly-interacting bosons^{29,30}. Following the frame work of the Bogoliubov theory, we assume the wave function has the following form:

$$\psi_L(\mathbf{x}, t) = \left[\psi_L^{pu} + u(\tilde{\epsilon})e^{-i(\tilde{\epsilon}/\hbar)t} e^{i\mathbf{k}\mathbf{x}} + v^*(\tilde{\epsilon})e^{i(\tilde{\epsilon}/\hbar)t} e^{-i\mathbf{k}\mathbf{x}} \right] \times e^{-i(\varepsilon_{pu}/\hbar)t}, \quad (27)$$

where u and v^* are the counterpropagating modes coupled by the polariton-polariton interaction, and ψ_L^{pu} is the “condensate” at $\mathbf{k} = \mathbf{0}$. Substituting Eq. 26 and 27 into the Gross-Pitaevskii equation Eq. 25 and keeping only terms that involve the condensate (Bogoliubov approximation), we obtain the following equations for $u(\tilde{\epsilon})$ and $v(\tilde{\epsilon})$ as

Fock-like (exchange) contributions, which are diagram-

matically represented in Fig. 2 (a) and (b)^{31,32}. On the other hand, the off-diagonal matrix elements $\alpha_1\psi_L^{pu2}$ and $-\alpha_1\psi_L^{pu2*}$ are the terms associated with the scattering of lower polaritons between \mathbf{k} and $-\mathbf{k}$ momentum states. In the terminology of non-linear optics, these processes correspond to a four-wave mixing process, which are also diagrammatically presented in Fig. 2 (c) and (d)^{31,32}. These three processes contribute to the probe pulse transmission spectrum. The solution for $u(\tilde{\epsilon})$ and $v(\tilde{\epsilon})$ are easily obtained respectively as

$$u(\tilde{\epsilon}) = \frac{\tilde{\epsilon} + (\epsilon_L - \epsilon_{pu} + \frac{\hbar^2 \mathbf{k}^2}{2m_L} + 2\alpha_1|\psi_L^{pu}|^2) - i\gamma_L}{D(\tilde{\epsilon})} |F^{pr}| \quad (29)$$

and

$$v(\tilde{\epsilon}) = -\frac{\alpha_1\psi_L^{pu*2}}{D(\tilde{\epsilon})} |F^{pr}|. \quad (30)$$

Here, $D(\tilde{\epsilon})$ is the determinant of the matrix in Eq. 28, which is given by

$$D(\tilde{\epsilon}) = \left[\tilde{\epsilon} - (\epsilon_L - \epsilon_{pu} + \frac{\hbar^2 \mathbf{k}^2}{2m_L} + 2\alpha_1|\psi_L^{pu}|^2) + i\gamma_L \right] \times \left[\tilde{\epsilon} + (\epsilon_L - \epsilon_{pu} + \frac{\hbar^2 \mathbf{k}^2}{2m_L} + 2\alpha_1|\psi_L^{pu}|^2) - i\gamma_L \right] + \alpha_1^2 |\psi_L^{pu}|^4. \quad (31)$$

Remembering that the probe $\psi_L^{pr}(\epsilon)$ and the four-wave mixing (idler) signal $\psi_L^{id}(\epsilon)$ are the responses of the system at \mathbf{k} and $-\mathbf{k}$ respectively, they are given by

$$\psi_L^{pr}(\epsilon) = u(\epsilon - \epsilon_{pu}) e^{-i(\epsilon/\hbar)t} \quad (32)$$

and

$$\psi_L^{id}(\epsilon) = v^*(\epsilon - \epsilon_{pu}) e^{-i((2\epsilon_{pu} - \epsilon)/\hbar)t}, \quad (33)$$

where we used $\tilde{\epsilon} = \epsilon - \epsilon_{pu}$. Setting $\gamma_L = 0$, the peak energies of the probe pulse transmission resonances are easily calculated as

$$\epsilon^\pm = \epsilon_L \pm \sqrt{(\epsilon_L - \epsilon_{pu} + \frac{\hbar^2 \mathbf{k}^2}{2m_L} + 2\alpha_1|\psi_L^{pu}|^2)^2 - \alpha_1^2 |\psi_L^{pu}|^4}. \quad (34)$$

ϵ^+ and ϵ^- respectively correspond to the normal branch and the so-called "ghost branch"^{5,6,33}. Due to the numerator of Eq. 29, the amplitude of the ghost branch is much weaker than that of the normal branch in the probe spectrum³³. Experimentally, the ghost branch is only visible in the four-wave mixing signal^{5,6,33,34}. Therefore, in our pump-probe spectroscopy, let us consider only the normal branch. When the in-plane momentum of the probe beam is small enough ($\mathbf{k} \simeq 0$) and the energy of the pump beam is resonant to the lower polariton branch

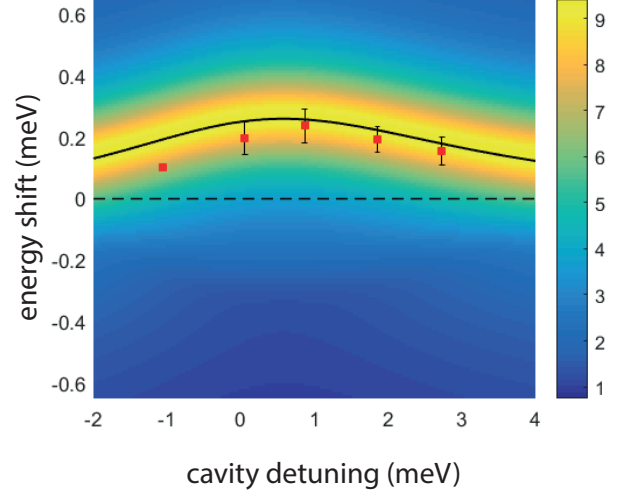


FIG. 3. Probe polariton peak spectrum $|\psi_L^{pr}(\epsilon - \epsilon_L)|/|F^{pr}|$ is plotted as a function of the cavity detuning for a co-circularly polarized pump-probe configuration. The red filled squares are experimentally measured energy shifts of the probe peak. The solid black curve represents ΔE_{co} (Eq. 35).

($\epsilon_{pu} = \epsilon_L$), from Eq. 34, the normal branch energy shift of the probe spectrum is given by

$$\Delta E_{co} = \sqrt{3}\alpha_1|\psi_L^{pu}|^2. \quad (35)$$

We note that the Hartree-like, Fock-like and four-wave mixing contributions magnify the blue shift of the probe polariton by a factor of $\sqrt{3}$. The Hartree-like and Fock-like terms enhance the blue shift by a factor of two, but the population loss due to the four-wave mixing signal generation reduces the enhancement to $\sqrt{3}$. In Fig. 3, the red filled squares are the experimentally extracted probe peak energy shifts at five different cavity detunings. The theoretical probe spectrum $|\psi_L^{pr}(\epsilon - \epsilon_L)|/|F^{pr}|$ is also plotted as a function of the cavity detuning. Here we assume that the pump polariton population depends on the cavity detuning as $|\psi_L^{pu}|^2 = |C_0|^2 n_{ext}^{pu}$, where n_{ext}^{pu} is proportional to the photon number of the pump pulse used in the experiment. As presented in Fig. 3, with the increase of the cavity detuning, the energy shift becomes larger and reaches a maximum at a cavity detuning of 1 meV. This is because the lower-polariton becomes more excitonic. However, as the cavity detuning increases further, the energy shift starts to decrease, because, following $|C_0|^2$, the coupling between lower-polaritons and the photon field outside the cavity becomes weaker.

B. Pump-probe spectroscopy with counter-circularly polarized lights

Now, let us consider the case when the pump and probe pulses are counter-circularly polarized. Since in this configuration a biexciton formation is allowed, we take into

account the biexciton state wave function and polariton-biexciton coupling. In this section, we investigate the scattering resonance of polaritons with a biexciton within a mean-field two-channel model^{12,16,18}. We consider the case where the system is driven by a strong spin-down pump and probed by a weak spin-up probe. Let us assume spin-up and spin-down polariton wave-functions respectively as

$$\psi_{L,\uparrow} = \psi_{L,\uparrow}^{pr} = u_{\uparrow}(\tilde{\epsilon}) e^{-i(\tilde{\epsilon} + \varepsilon_{pu})t/\hbar} e^{i\mathbf{k}\mathbf{x}} \quad (36)$$

and

$$\psi_{L,\downarrow} = \psi_{L,\downarrow}^{pu} e^{-i\varepsilon_{pu}t/\hbar}. \quad (37)$$

Here, the biexciton wave-function is assumed to be

$$\psi_B = m(\tilde{\epsilon}) e^{-i(\tilde{\epsilon} + 2\varepsilon_{pu})t/\hbar} e^{i\mathbf{k}\mathbf{x}}. \quad (38)$$

The input probe beam is set as

$$f_{ext}^{pr} = |F_{\uparrow}^{pr}| e^{-i(\tilde{\epsilon} + \varepsilon_{pu})t/\hbar} e^{i\mathbf{k}\mathbf{x}}. \quad (39)$$

Substituting these into the spinor Gross-Pitaevskii equations Eq. 23 and 24, we obtain equations for $u_{\uparrow}(\tilde{\epsilon})$ and $m(\tilde{\epsilon})$ as

$$\begin{pmatrix} \tilde{\epsilon} - (\varepsilon_L - \varepsilon_{pu} + \frac{\hbar^2 \mathbf{k}^2}{2m_L} + g_L^{+-} |\psi_{L,\downarrow}^{pu}|^2) + i\gamma_L & -g_L^{bx} \psi_{L,\downarrow}^{pu*} \\ -g_L^{bx} \psi_{L,\downarrow}^{pu} & \tilde{\epsilon} - (\varepsilon_B - 2\varepsilon_{pu} + \frac{\hbar^2 \mathbf{k}^2}{2m_B}) + i\gamma_B \end{pmatrix} \begin{pmatrix} u_{\uparrow}(\tilde{\epsilon}) \\ m(\tilde{\epsilon}) \end{pmatrix} = \begin{pmatrix} |F_{\uparrow}^{pr}| \\ 0 \end{pmatrix}. \quad (40)$$

The energy shift term due to the background polariton interaction with anti-parallel spins $g_L^{+-} |\psi_{L,\downarrow}^{pu}|^2$ is diagrammatically represented in Fig. 4 (a). We note that the Fock-like (exchange) term does not exist in g^{+-} , because the spin-up and spin-down polaritons cannot exchange indistinguishably. Additionally, the polariton-biexciton coupling $g_L^{bx} \psi_{L,\downarrow}^{pu}$ and $g_L^{bx} \psi_{L,\downarrow}^{pu*}$ are shown by the diagram Fig. 4 (b) and (c) respectively. Using the determinant of the matrix in Eq. 40:

$$\begin{aligned} D^{+-}(\tilde{\epsilon}) &= \left[\tilde{\epsilon} - (\varepsilon_L - \varepsilon_{pu} + \frac{\hbar^2 \mathbf{k}^2}{2m_L} + g_L^{+-} |\psi_{L,\downarrow}^{pu}|^2) + i\gamma_L \right] \\ &\times \left[\tilde{\epsilon} - (\varepsilon_B - 2\varepsilon_{pu} + \frac{\hbar^2 \mathbf{k}^2}{2m_B}) + i\gamma_B \right] \\ &- g_L^{bx2} |\psi_{L,\downarrow}^{pu}|^2, \end{aligned} \quad (41)$$

the solution is easily found for $u_{\uparrow}(\tilde{\epsilon})$ as

$$u_{\uparrow}(\tilde{\epsilon}) = \frac{\tilde{\epsilon} - (\varepsilon_B - 2\varepsilon_{pu} + \frac{\hbar^2 \mathbf{k}^2}{2m_B}) + i\gamma_B}{D^{+-}(\tilde{\epsilon})} |F_{\uparrow}^{pr}|. \quad (42)$$

For $m(\tilde{\epsilon})$, the solution is

$$m(\tilde{\epsilon}) = \frac{g_L^{bx} \psi_{L,\downarrow}^{pu}}{D^{+-}(\tilde{\epsilon})} |F_{\uparrow}^{pr}|. \quad (43)$$

Using $\tilde{\epsilon} = \epsilon - \varepsilon_{pu}$, the probe polariton wave-function is represented as

$$\begin{aligned} \psi_{L,\uparrow}^{pr}(\epsilon) &= u_{\uparrow}(\epsilon - \varepsilon_{pu}) e^{-i(\epsilon/\hbar)t} \\ &= |F_{\uparrow}^{pr}| e^{-i(\epsilon/\hbar)t} \\ &\times \left[\epsilon - (\varepsilon_L + \frac{\hbar^2 \mathbf{k}^2}{2m_L} + g_L^{+-} |\psi_{L,\downarrow}^{pu}|^2) + i\gamma_L \right. \\ &\left. - \frac{g_L^{bx2} |\psi_{L,\downarrow}^{pu}|^2}{\epsilon - (\varepsilon_B - \varepsilon_{pu} + \frac{\hbar^2 \mathbf{k}^2}{2m_B}) + i\gamma_B} \right]^{-1} \end{aligned} \quad (44)$$

The above expression indicates that a resonance occurs when the sum of the energy of the pump and probe lower-polariton ($\varepsilon_{pu} + \epsilon$) coincides with that of the biexciton (ε_B), which is interpreted as a polaritonic version of the Feshbach resonance in cold atoms^{9,12,16}. Furthermore, there are two solutions corresponding to the two eigenenergies of the probe polariton states $\psi_{L,\uparrow}^{pr}$. Setting $\gamma_L = 0$ and $\gamma_B = 0$, the two peak energies are given by

$$\begin{aligned} \epsilon_{cr}^{\pm} &= \frac{1}{2} (\varepsilon_L + \frac{\hbar^2 \mathbf{k}^2}{2m_L} + \varepsilon_B + \frac{\hbar^2 \mathbf{k}^2}{2m_B} - \varepsilon_{pu} + g_L^{+-} |\psi_{L,\downarrow}^{pu}|^2) \\ &\pm \frac{1}{2} \left[(\varepsilon_L + \frac{\hbar^2 \mathbf{k}^2}{2m_L} - \varepsilon_B - \frac{\hbar^2 \mathbf{k}^2}{2m_B} + \varepsilon_{pu} \right. \\ &\left. + g_L^{+-} |\psi_{L,\downarrow}^{pu}|^2)^2 + 4g_L^{bx2} |\psi_{L,\downarrow}^{pu}|^2 \right]^{\frac{1}{2}}. \end{aligned} \quad (45)$$

Figure. 5 (a) presents the experimental energy shift of the probe peak as red filled squares at five different values of the detuning. The spectrum of the probe polariton $|\psi_{L,\uparrow}^{pr}(\epsilon - \varepsilon_L)|/|F_{\uparrow}^{pr}|$ is also overlapped in Fig. 5 (a) as a function of the cavity detuning. The pump beam photon number n_{ext}^{pu} is identical to the co-circular polarization configuration (Fig. 3) and we assume $|\psi_{L,\downarrow}^{pu}|^2 = |C_0|^2 n_{ext}^{pu}$.

Supposing a small in-plane momentum of the probe polariton $\mathbf{k} = 0$ and the pump beam resonant to the lower-polariton $\varepsilon_{pu} = \varepsilon_L$, from Eq. 45, we obtain energy shifts of the probe as

$$\begin{aligned} \Delta\epsilon_{cr}^{\pm} &= -\varepsilon_L + \frac{1}{2} (g_L^{+-} |\psi_{L,\downarrow}^{pu}|^2 + \varepsilon_B) \\ &\pm \frac{1}{2} \sqrt{(g_L^{+-} |\psi_{L,\downarrow}^{pu}|^2 - \varepsilon_B + 2\varepsilon_L)^2 + 4g_L^{bx2} |\psi_{L,\downarrow}^{pu}|^2}. \end{aligned} \quad (46)$$

When the dephasing rate of the biexciton is large, which is the case in our system, we approximate the two modes

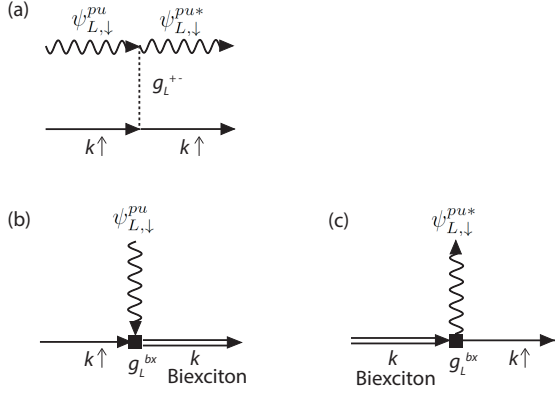


FIG. 4. Diagrammatic representation of polariton interaction with anti-parallel spins. Solid lines represent spin-up probe polaritons with momentum \mathbf{k} (right arrow), which is injected by the weak probe beam with σ^+ circular polarization. The wavy lines represent condensates of the spin-down lower polaritons with zero momentum, which is driven by the strong pump beam with a σ^- circular polarization. The dashed line represent the polariton-polariton interaction with anti-parallel spins g_L^{+-} . The double line is a biexciton. (a) Hartree-like (direct) process. The association (b) and dissociation (c) of a biexciton via the polariton-biexciton coupling g_L^{bx} .

eigenstates as a single solution by putting $\epsilon = \epsilon^{pu} = \epsilon_L$ into the denominator of the resonance term in Eq. 44. Then, the energy shift of the lower-polariton mode at $\mathbf{k} = 0$ is approximated as

$$\Delta E_{cr} \simeq g_L^{+-} |\psi_{L,\downarrow}^{pu}|^2 + \text{Re} \left[\frac{g_L^{bx2} |\psi_{L,\downarrow}^{pu}|^2}{2\epsilon_L - \epsilon_B + i\gamma_B} \right]. \quad (47)$$

Now, let us define a complex interaction constant $\alpha_2 - i\alpha'_2$ based on Eq. 47. The real and imaginary parts are respectively defined as

$$\alpha_2 = g_L^{+-} + g_L^{bx2} \frac{2\epsilon_L - \epsilon_B}{(2\epsilon_L - \epsilon_B)^2 + \gamma_B^2} \quad (48)$$

and

$$\alpha'_2 = g_L^{bx2} \frac{\gamma_B}{(2\epsilon_L - \epsilon_B)^2 + \gamma_B^2}. \quad (49)$$

While the energy shift of the probe spectrum is associated with α_2 , the imaginary part of the effective interaction α'_2 contributes to the pump induced suppression (absorption) of the spectral peak through the large biexciton decay rate γ_B . In Appendix. C, we discuss that this effective interaction constant α_2 is directly obtained from the polariton-biexciton coupling Hamiltonian using a canonical transformation and interpreted as a second-order perturbation. The reduction of the spectral peak amplitude is represented as an absorbance in Fig. 5 (b), which measure $\ln(A_{\max}^{\text{ref}}/A_{\max}^{\text{pp}})$. A_{\max}^{ref} and A_{\max}^{pp} are maximum heights of the measured probe spectrum without and with the pump beam respectively (See the inset in

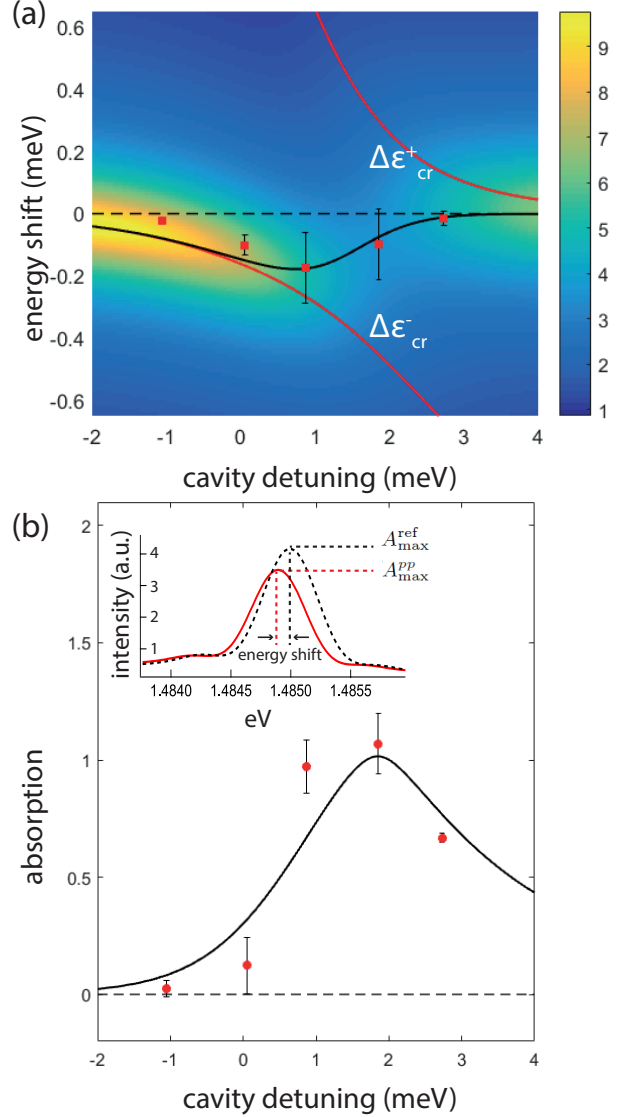


FIG. 5. Peak energy shift and probe pulse transmission intensity for a cross-circularly polarized pump-probe configuration. (a) The filled red squares are measured probe peak energy shifts. Probe spectrum $|\psi_{L,\uparrow}^{pr}(\epsilon - \epsilon_L)|/|F_{\uparrow}^{pr}|$ is plotted as a function of the cavity detuning. Two red lines represent the energy shifts expressed as $\Delta\epsilon_{cr}^{\pm}$ (Eq. 46), while the black line is the approximated energy shift ΔE_{cr} (Eq. 47). (b) The filled red squares are measured peak absorbance. The solid black line represents the simulated absorbance based on the theoretical model. The inset presents the experimental probe spectrum with (red line) and without the pump beam (black dashed line) at the cavity detuning $\delta = 0.05$ meV.

Fig. 5 (b)). The solid curve in Fig. 5 (b) is the theoretical prediction based on the solution given by Eq. 44. Fig. 5 (b) evidences a clear maximum of the absorption for a detuning around 2 meV, which is the consequence of the decay of polaritons through the biexciton channel. The polaritonic Feshbach resonance might be analogous to the optical Feshbach resonance in the cold atom physics. In the conventional magnetic field induced Feshbach res-

onance, the lifetime of molecules is very long and the interaction strength diverges. In contrast, in an optical Feshbach resonance, a large loss of atoms is observed through the molecular decay channel and prevents the interaction strength from diverging³⁵. The large γ_B might be associated with the spontaneous dissociation channel of the biexciton into two polaritons to all momentum combinations satisfying the energy-momentum conservation, which is neglected in Fig. 4 (c). Finally, we would like to comment on the necessity of the background attractive interaction g_L^{+-} . Figure. 5 (a) presents the offset of the dispersive curve, which is explained phenomenologically with an additional background interaction. We discuss the physical origin of this background interaction in Appendix B.

C. Extraction of interaction constants and spinor interaction ratio α_2/α_1

The physical parameters employed in the numerical plots of Fig. 3 and 5 are extracted by fitting the model to the experiments. The fitting is performed in an automatic way by applying the least-square method to the energy shifts of co- and counter-circular polarization configuration, the absorbance, and the ratio α_2/α_1 simultaneously. For the fitting, we fix the exciton-exciton interaction constant g as a unity ($g \equiv 1$), then the pump photon density is found to be $n_{\text{ext}}^{pu} = 0.53$. The extracted interaction constants are scaled with respect to the value of g : i.e., the polariton interaction constants $g^{+-} = -1.19g$ and $g^{bx} = 1.37g\sqrt{n_{\text{ext}}^{pu}}$. The extracted biexciton energy and dephasing rate are respectively $\varepsilon_B = 2\varepsilon_x - 2.13$ meV and $\gamma_B = 0.80$ meV. On the other hand, for simplicity, we fix the photon assisted exchange scattering strength and lower-polariton dephasing rate as $g_{\text{pae}} = 0.3g$ and $\gamma_L = 0.1$ meV respectively³⁶. The parameters used for the theoretical plots are summarized in Table. I

TABLE I. Parameters used for the theoretical curves. The binding energy of the biexciton ε_{bin} is defined as $\varepsilon_{\text{bin}} = 2\varepsilon_x - \varepsilon_B$. The parameters g , g_{pae} , and γ_L have fixed values.

g	g_{pae}	g^{+-}	g^{bx}	γ_L	γ_B	ε_{bin}	n_{ext}^{pu}
	(g)	(g)	($g\sqrt{n_{\text{ext}}^{pu}}$)	(meV)	(meV)	(meV)	
1	0.3	-1.19	1.37	0.1	0.80	2.13	0.53

Finally, we present the ratio between polariton interaction with parallel and with anti-parallel spins. Using the effective interaction constant α_2 defined in Eq. 48 and α_1 in Eq. 19, the ratio of the polariton interaction α_2/α_1 is shown in Fig. 6. Experimentally, the ratio of the interactions is obtained from the energy shifts as $\alpha_2/\alpha_1 = \sqrt{3}\Delta E_{\text{exp}}^{cr}/\Delta E_{\text{exp}}^{co}$, where $\Delta E_{\text{exp}}^{co(cr)}$ is the measured probe energy shift in the co (counter)-circularly polarized pump-probe configuration presented in Fig. 3 (Fig. 5). The factor $\sqrt{3}$ is necessary because of enhancement of the probe energy shift $\Delta E_{\text{exp}}^{co}$ (Eq. 35). An im-

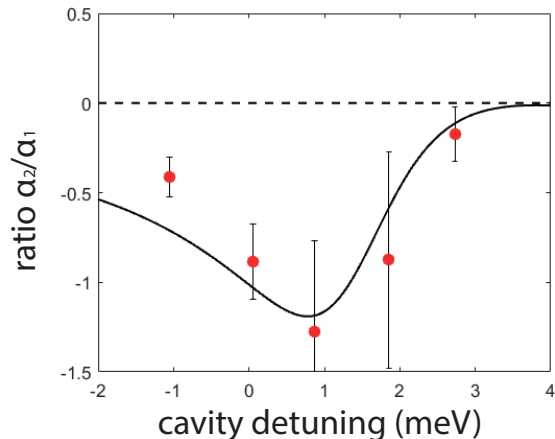


FIG. 6. The ratio of the effective interaction constants of lower-polaritons with anti-parallel and parallel spins α_2/α_1 as a function of the cavity detuning. The solid line is the plot based on the theoretical model.

portant consequence of the cavity detuning dependence of the ratio α_2/α_1 is that the lower-polariton interaction with anti-parallel spins enhances dramatically and becomes comparable to that of parallel spins in the vicinity of the biexciton resonance^{11,18}. This indicates that the collapse of Bose-Einstein condensates of polaritons might be possible at positive cavity detuning¹¹. However, we stress that in the proximity of the scattering resonance the enhanced non-linear decay is not negligible, which is associated with the imaginary part of the interaction constant α_2' . Even though the enhancement of α_2 is not as dramatic as the Feshbach resonance in cold atoms, the large dissipative nonlinearity α_2' is still useful in the non-equilibrium system for some applications such as non-classical photon generation¹⁰ and polariton spin switching³⁷. Actually, the use of the dissipative nonlinearity is pointed out in the context of a polariton blockade¹⁰. Another interesting direction of investigation on the large biexciton decay rate is a source of entangled photons. As discussed in the previous subsection, the large decay rate of the biexciton might originate from the spontaneous dissociation channel into two polaritons. As predicted in Ref¹⁴, the biexciton will emit entangled polaritons (or photons outside the microcavity) with anti-parallel spins (with counter-circular polarizations) in its radiative decay.

V. CONCLUSION

We investigated spinor interactions of lower-polaritons in semiconductor microcavities employing a pump-probe technique with a spectrally narrow pulse. The analysis of the stationary properties of interacting lower-polaritons was performed with the Bogoliubov theory and a mean-field two-channel model. We observe a large enhancement of the interaction strength with the lower polaritons

in the vicinity of the resonance given by the generation of a biexciton from the scattering with two polaritons with opposite spins. This phenomenon can be interpreted as a polaritonic version of the Feshbach resonance in cold atom physics. Furthermore, the ratio between the lower-polariton interaction with parallel (α_1) and anti-parallel spins (α_2) indicates that α_2 can be comparable to α_1 in the proximity of this scattering resonance.

ACKNOWLEDGMENTS

The present work is supported by the Swiss National Science Foundation under Project No. 153620 and the European Research Council under project Polaritonics, Contract No. 291120. The polatom network is also acknowledged.

APPENDIX A: SPINOR POLARITON DYNAMICS

In the main text, the pump-probe time delay is fixed to zero and only the stationary properties of spinor polaritons are investigated. Here we investigate the dynamical aspects of the spinor polaritons. The dynamical properties of the polariton-biexciton coupling system is interesting concerning the real time formation of the biexcitons in the vicinity of the polaritonic Feshbach resonance. Moreover, the time delay dependence of the pump-probe spectra provides the response time of the non-linearity, which would determine the switching speed of polaritonic devices. Figure 7 presents probe spectra as a function of the pump-probe time delay for three different cavity detunings: below (a), on (b), and above the resonance (c) with the biexciton. In order to simulate the dynamical properties, the simplest approach is to numerically integrate the spinor Gross-Pitaevskii equations with biexciton (Eq. 23 and 24). Coupled mode equations for the probe, pump, and biexciton are written as

$$i\hbar\dot{\psi}_{L,\uparrow}^{pr}(t) = \left[\varepsilon_L - i\gamma_L + \alpha_1 |\psi_{L,\uparrow}^{pr}(t)|^2 + g_L^{+-} |\psi_{L,\downarrow}^{pu}(t)|^2 \right] \psi_{L,\uparrow}^{pr}(t) + g_L^{bx} \psi_B(t) \psi_{L,\downarrow}^{pu*}(t) + f_{ext,\uparrow}^{pr}(t), \quad (50)$$

$$i\hbar\dot{\psi}_{L,\downarrow}^{pu}(t) = \left[\varepsilon_L - i\gamma_L + \alpha_1 |\psi_{L,\downarrow}^{pu}(t)|^2 + g_L^{+-} |\psi_{L,\uparrow}^{pr}(t)|^2 \right] \psi_{L,\downarrow}^{pu}(t) + g_L^{bx} \psi_B(t) \psi_{L,\uparrow}^{pr*}(t) + f_{ext,\downarrow}^{pu}(t) \quad (51)$$

and,

$$i\hbar\dot{\psi}_B(t) = (\varepsilon_B - i\gamma_B) \psi_B(t) + g_L^{bx} \psi_{L,\uparrow}^{pr}(t) \psi_{L,\downarrow}^{pu}(t). \quad (52)$$

The driving pump (probe) fields are written as a Gaussian pulse:

$$f_{ext,\downarrow(\uparrow)}^{pu(pr)} = F^{pu(pr)} \exp \left[-\frac{(t - t_{pu(pr)})^2}{2\tau_{pu(pr)}^2} \right] \cdot \exp \left[-i \frac{\varepsilon_{pu(pr)}}{\hbar} (t - t_{pu(pr)}) \right]. \quad (53)$$

We set the pulse durations as $\tau_{pu} = 1.5$ ps and $\tau_{pr} = 0.35$ ps. The setting of the pulse intensities are $|F^{pu}|^2 = 0.16$ and $|F^{pr}|^2 = 0.03$. Simulated probe spectra based on the above equations are shown in Fig. 8 (a)-(c). All interaction constants used for the simulations in Fig. 8 is same as those used for the stationary model in the main text. As we expect, this set of equations reproduces the basic features of the polaritonic Feshbach resonance (energy shift and absorption of the probe polariton induced by the biexciton). However, there are striking differences between the experiments and simulations in the pump-probe delay dependence. In particular, the simulation does not reproduce the positive pump-probe delay part of the observed spectra. This is due to the fact that the model used here is fully coherent and neglects any long-lived population beyond the cavity lifetime. Inspired by previous works^{19,38,39}, we try to construct phenomenologically a set of coupled mode equations including an exciton reservoir:

$$i\hbar\dot{\psi}_{L,\uparrow}^{pr}(t) = \left[\varepsilon_L - i\gamma_L + (\alpha_{2C} - i\alpha'_{2C}) \cdot |\psi_{L,\downarrow}^{pu}(t)|^2 + (\alpha_{2R} - i\alpha'_{2R}) \cdot n_{R,\downarrow}(t) \right] \psi_{L,\uparrow}^{pr}(t) + f_{ext,\uparrow}^{pr}(t), \quad (54)$$

$$i\hbar\dot{\psi}_{L,\downarrow}^{pu}(t) = \left[\varepsilon_L - i\gamma_L + (\alpha_{1C} - i\alpha'_{1C}) \cdot |\psi_{L,\downarrow}^{pu}(t)|^2 + (\alpha_{1R} - i\alpha'_{1R}) \cdot n_{R,\downarrow}(t) \right] \psi_{L,\downarrow}^{pu}(t) + f_{ext,\downarrow}^{pu}(t), \quad (55)$$

and

$$\hbar\dot{n}_{R,\downarrow}(t) = -\gamma_R n_{R,\downarrow}(t) + 2\alpha'_{1C} |\psi_{L,\downarrow}^{pu}(t)|^4, \quad (56)$$

where $n_{R,\downarrow}$ is the spin-down reservoir population and a long lifetime is assumed $\gamma_R = 0.01$ meV¹⁹. Here we neglect the spin-up incoherent reservoir and the coherent population, because the weak spin-up probe pulse creates only a small amount of spin-up incoherent reservoir and coherent population. In this approach, we do not include the biexciton degree of freedom, instead, the effect of biexciton resonance is indirectly included in the effective complex interaction constants $\alpha_{2C(R)}$ and $\alpha'_{2C(R)}$. In addition to this, we also introduce a complex interaction constant $\alpha_{1C(R)} + i\alpha'_{1C(R)}$ for the polaritons with parallel spins. The imaginary part $\alpha'_{1C(R)}$ represents excitation induced dephasing (EID), which converts the coherent polariton population into the incoherent population¹⁹. The symbol C and R represent the

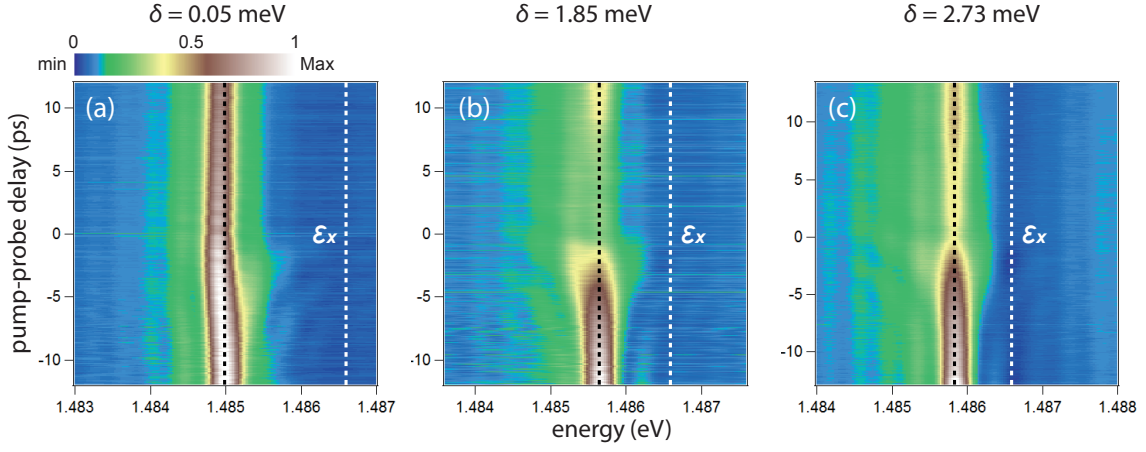


FIG. 7. Experimental probe spectrum as a function of the pump-probe delay for the cavity detuning: 0.05 meV (a), 1.85 meV (b), and 2.73 meV (c). The black dashed lines represent the lower polariton peak energies without pump pulse. The exciton energy is represented as the white dashed line. The color scale is normalized by the lower-polariton branch.

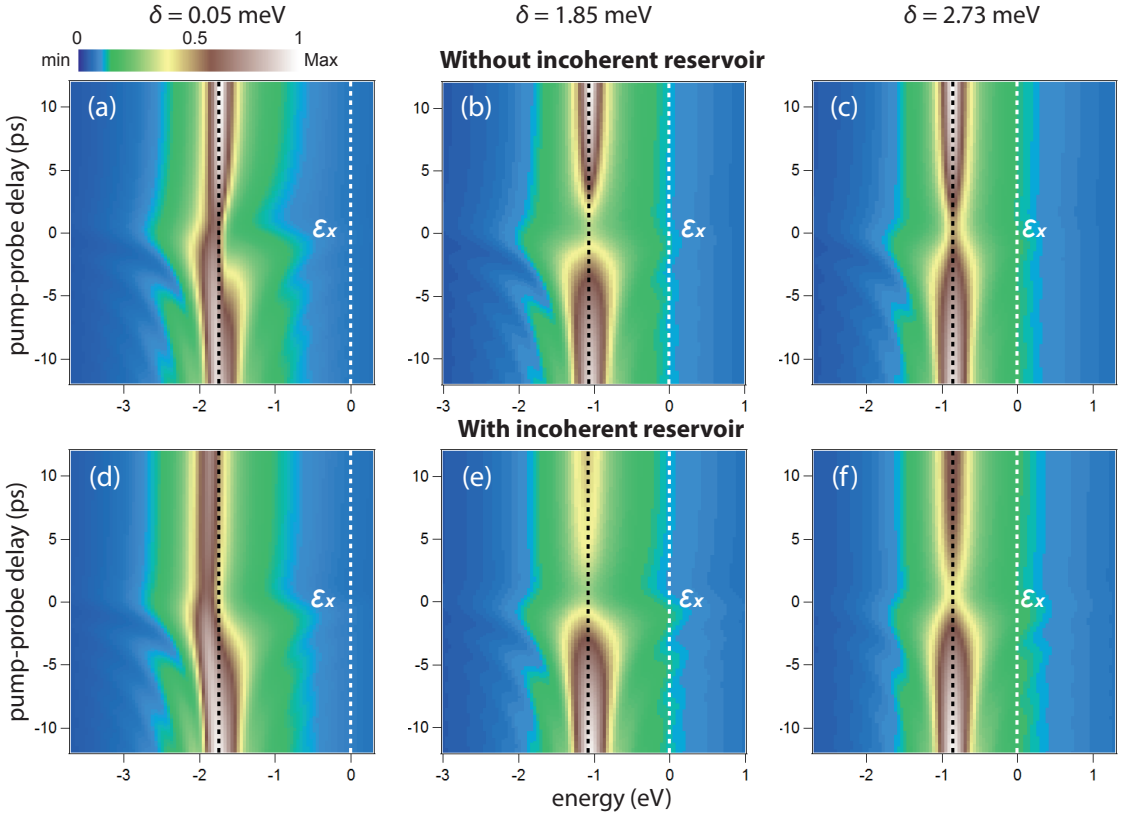


FIG. 8. Simulated probe spectrum based on the coherent polariton-biexciton Gross-Pitaevskii equations as a function of the pump-probe time delay. The cavity detunings are 0.05 meV (a,d), 1.85 meV (b,e), and 2.73 meV (c,f). The black dashed lines represent the lower polariton peak energies without pump pulse. The exciton energy is represented as the white dashed line. The color scale is normalized by the lower-polariton branch.

contributions to the mean field energy shift from coherent polaritons and incoherent reservoir respectively. In this appendix, for simplicity, we chose $\alpha_{1C}^{(l)} = \alpha_{1R}^{(l)} = \alpha_1^{(l)}$ and $\alpha_{2C}^{(l)} = \alpha_{2R}^{(l)} = \alpha_2^{(l)}$. Following our previous work¹⁹, we set $\alpha_1' = 0.3g$. In this condition, the mean field energy shift is simply proportional to the total population such as $\alpha_{1(2)}N_{\downarrow}$, where the total population N_{\downarrow} is given

by $N_{\downarrow} = |\psi_{L,\downarrow}^{pu}|^2 + n_{R,\downarrow}$. We stress that this choice is just a one of the possible choices of the coherent and incoherent interaction constants that can qualitatively reproduce the experimental results. Numerical simulations are presented in Fig. 8 (d-f), which reproduce the positive pump-probe delay region of the probe spectra much better than the previous fully coherent model. In the positive pump-probe time delay part, the energy-shift and

absorption of the probe polariton survives more than 10 ps. This is because the decay of the coherent spin-down polariton population is compensated by the long-lived spin-down incoherent population in the reservoir, that is induced by EID. In other words, the long lived energy-shift and the reduction of the polariton absorption at positive pump-probe delays are associated with the coupling between the incoherent reservoir and biexciton⁴⁰. On the other hand, the negative pump-probe delay part of the spectrum mainly evidences a coherent coupling between polaritons and biexcitons⁴¹. Although the incoherent reservoir model phenomenologically reproduces the experimental delay dependent pump-probe spectra, a further investigation is required in order to understand the true character and the creation mechanism of the reservoir¹⁹. In particular, since two lower-polaritons with low in-plane momenta energetically cannot scatter to a large in-plane momentum exciton reservoir, the nature of the reservoir is not clear. One should consider the scattering process of a lower polariton from the pump pulse with an upper polariton from the probe pulse to the reservoir of excitons in order to account for the absorption change at the spectral position of the lower polariton resonance. Even if we consider this process we cannot explain the existence of a long lived reservoir. In the view point of the design of polaritonic devices, since the long lifetime of the reservoir ($\hbar/\gamma_R \sim 66$ ps) limits the response time, we should minimize the reservoir creation by choosing appropriate experimental conditions: a low enough excitation power and a cavity detuning away from the biexciton resonance and EID.

APPENDIX B: EXCITON SCATTERING CONTINUUM AND BACK GROUND INTERACTION

In this appendix, we discuss how the background interaction appears from a bare exciton-exciton interaction. In general, using a non-contact potential $W^{+-}(\mathbf{x})$ and field operators of excitons, the bare exciton-exciton interaction is expressed as

$$\begin{aligned} \hat{W}^{+-} &= \int d\mathbf{x} \left[\hat{\psi}_{x,\uparrow}^\dagger \hat{\psi}_{x,\downarrow}^\dagger W^{+-}(\mathbf{x} - \mathbf{x}') \hat{\psi}'_{x,\downarrow} \hat{\psi}_{x,\uparrow} \right] \\ &= \sum_{\mathbf{k}\mathbf{k}'\mathbf{q}} \tilde{W}^{+-}(\mathbf{q}) \hat{x}_{\mathbf{k}-\mathbf{q},\uparrow}^\dagger \hat{x}_{\mathbf{k}'+\mathbf{q},\downarrow}^\dagger \hat{x}_{\mathbf{k}',\downarrow} \hat{x}_{\mathbf{k},\uparrow}. \end{aligned} \quad (57)$$

Here $\hat{x}_{\mathbf{k},\sigma}$ is an exciton annihilation operator. The exciton annihilation operator $\hat{x}_{\mathbf{k},\sigma}$ and the exciton field operator $\hat{\psi}_{x,\sigma}(\mathbf{x})$ are related as

$$\hat{\psi}_{x,\sigma}(\mathbf{x}) = \sum_{\mathbf{k}} \frac{1}{\sqrt{S}} e^{i\mathbf{k}\cdot\mathbf{x}} \cdot \hat{x}_{\mathbf{k},\sigma}, \quad (58)$$

where S is the area occupied by excitons. $\tilde{W}^{+-}(\mathbf{q})$ is defined with the Fourier transformation as

$$\tilde{W}^{+-}(\mathbf{q}) = \int W^{+-}(\mathbf{x}) e^{-i\mathbf{q}\cdot\mathbf{x}} d\mathbf{x} \quad (59)$$

Importantly, the exciton-exciton interaction matrix $\tilde{W}^{+-}(\mathbf{q})$ depends on momentum, which is the consequence of the non-contact interaction. Our objective is to find an effective interaction constant which does not depend on momentum. We need to find an effective interaction which reproduces the same scattering amplitude as the bare exciton-exciton interaction. In the three dimensional case, this procedure corresponds to replacing a momentum dependent bare interaction with a momentum independent scattering length^{23,42}. Since the scattering amplitude is connected to T-matrix, we evaluate the T-matrix using Lippman-Schwinger equation^{43,44}

$$\hat{T}(\epsilon) = \hat{W}^{+-} + \hat{W}^{+-} \frac{1}{\epsilon - \hat{H}_0} \hat{T}(\epsilon) \quad (60)$$

$$= \hat{W}^{+-} + \hat{W}^{+-} \frac{1}{\epsilon - \hat{H}^{+-}} \hat{W}^{+-}, \quad (61)$$

where \hat{H}_0 is the kinetic term of two excitons and $\hat{H}^{+-} = \hat{H}_0 + \hat{W}^{+-}$. Let us calculate the above T-matrix in terms of two-exciton basis defined as

$$|\mathbf{K}\mathbf{q}\rangle \equiv \hat{x}_{\mathbf{K}/2+\mathbf{q},\uparrow}^\dagger \hat{x}_{\mathbf{K}/2-\mathbf{q},\downarrow}^\dagger |0\rangle, \quad (62)$$

where the momentum \mathbf{K} and \mathbf{q} are respectively a center and a relative momentum given by

$$\mathbf{K} = \mathbf{k} + \mathbf{p} \quad (63)$$

and

$$\mathbf{q} = \frac{\mathbf{k} - \mathbf{p}}{2}, \quad (64)$$

where \mathbf{k} and \mathbf{p} are momenta of exciton with spin-up and -down, respectively. The T-matrix leads to

$$\begin{aligned} \langle \mathbf{K}\mathbf{q}_1 | \hat{T}(\epsilon) | \mathbf{K}\mathbf{q}_2 \rangle &= \langle \mathbf{K}\mathbf{q}_1 | \hat{W}^{+-} | \mathbf{K}\mathbf{q}_2 \rangle \\ &+ \langle \mathbf{K}\mathbf{q}_1 | \hat{W}^{+-} \frac{1}{\epsilon - \hat{H}^{+-}} \hat{W}^{+-} | \mathbf{K}\mathbf{q}_2 \rangle \\ &= \langle \mathbf{K}\mathbf{q}_1 | \hat{W}^{+-} | \mathbf{K}\mathbf{q}_2 \rangle \\ &+ \sum_{\mathbf{q}'\mathbf{q}''} \langle \mathbf{K}\mathbf{q}_1 | \hat{W}^{+-} | \mathbf{K}\mathbf{q}' \rangle \\ &\times \langle \mathbf{K}\mathbf{q}' | \frac{1}{\epsilon - \hat{H}^{+-}} | \mathbf{K}\mathbf{q}'' \rangle \\ &\times \langle \mathbf{K}\mathbf{q}'' | \hat{W}^{+-} | \mathbf{K}\mathbf{q}_2 \rangle \end{aligned} \quad (65)$$

The Hamiltonian \hat{H}^{+-} is generally expanded by two-exciton states as

$$\frac{1}{\epsilon - \hat{H}^{+-}} = \sum_n \frac{|B_{\mathbf{K}}^{(n)}\rangle \langle B_{\mathbf{K}}^{(n)}|}{\epsilon - \Omega_{\mathbf{K}}^{(n)}} \quad (66)$$

Using a two-exciton wave-function $\psi_B^{(n)}(\mathbf{K}, \mathbf{l})$, the nth two-exciton states $|B_{\mathbf{K}}^{(n)}\rangle$ is defined as

$$\begin{aligned} |B_{\mathbf{K}}^{(n)}\rangle &\equiv \sum_{\mathbf{l}} \psi_B^{(n)}(\mathbf{K}, \mathbf{l}) \hat{x}_{\mathbf{K}/2+\mathbf{l},\uparrow}^\dagger \hat{x}_{\mathbf{K}/2-\mathbf{l},\downarrow}^\dagger |0\rangle \\ &= \sum_{\mathbf{l}} \psi_B^{(n)}(\mathbf{K}, \mathbf{l}) |\mathbf{K}\mathbf{l}\rangle \end{aligned} \quad (67)$$

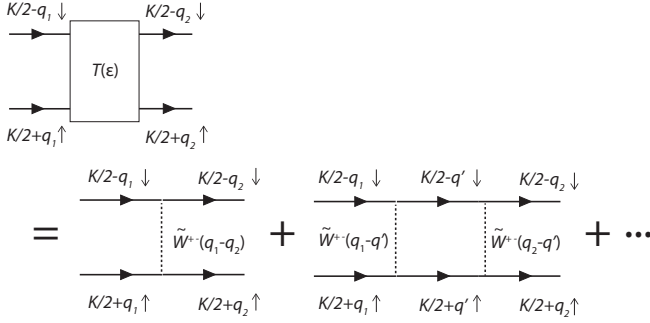


FIG. 9. Diagrammatic representation of the T-matrix.

The n th two-exciton wave-function $\psi_B^{(n)}(\mathbf{K}, \mathbf{l})$ and eigen energy $\Omega_{\mathbf{K}}^{(n)}$ satisfy a following two-bodies Schroedinger equation (also referred to as the Bethe-Salpeter equation)⁴⁵:

$$[\epsilon_{\frac{1}{2}\mathbf{K}+\mathbf{l}} + \epsilon_{\frac{1}{2}\mathbf{K}-\mathbf{l}}]\psi_B^{(n)}(\mathbf{K}, \mathbf{l}) + \sum_{\mathbf{l}'} \tilde{W}^{+-}(\mathbf{l}-\mathbf{l}')\psi_B^{(n)}(\mathbf{K}, \mathbf{l}') = \Omega_{\mathbf{K}}^{(n)}\psi_B^{(n)}(\mathbf{K}, \mathbf{l}), \quad (68)$$

where $\epsilon_{\frac{1}{2}\mathbf{K}\pm\mathbf{l}}$ is the energy of a free exciton. This equation indicates that if the exciton-exciton interaction potential $\tilde{W}^{+-}(\mathbf{q})$ is given, both wave-functions and eigen energies are uniquely determined. These calculation is out of scope of our article, but we refer to several works that attempted the estimations^{43,46}. Finally, the T-matrix Eq. 65 is simplified as

$$\langle \mathbf{K}\mathbf{q}_1 | \hat{T}(\epsilon) | \mathbf{K}\mathbf{q}_2 \rangle = \tilde{W}^{+-}(\mathbf{q}_1 - \mathbf{q}_2) + \sum_n \frac{g_{bx}^{(n)}(\mathbf{K}, \mathbf{q}_1, \mathbf{q}_2)}{\epsilon - \Omega_{\mathbf{K}}^{(n)}}, \quad (69)$$

where $g_{bx}^{(n)}$ represents⁴⁵

$$g_{bx}^{(n)}(\mathbf{K}, \mathbf{q}_1, \mathbf{q}_2) = \sum_{\mathbf{q}'\mathbf{q}''} \tilde{W}^{+-}(\mathbf{q}_1 - \mathbf{q}')\psi_B^{(n)}(\mathbf{K}, \mathbf{q}') \times \psi_B^{(n)*}(\mathbf{K}, \mathbf{q}'')\tilde{W}^{+-}(\mathbf{q}'' - \mathbf{q}_2) \quad (70)$$

Since we are interested in low momentum scattering, let us set $\mathbf{K} = \mathbf{0}$ and $\mathbf{q}_1 = \mathbf{q}_2 = \mathbf{0}$. The low momentum scattering amplitude reads:

$$\langle \mathbf{00} | \hat{T}(\epsilon) | \mathbf{00} \rangle = \tilde{W}^{+-}(\mathbf{0}) + \sum_n \frac{g_{bx}^{(n)}(\mathbf{0}, \mathbf{0}, \mathbf{0})}{\epsilon - \Omega_{\mathbf{0}}^{(n)}}. \quad (71)$$

In the first order Born approximation, the scattering amplitude is approximated with the lowest order term as $\langle \mathbf{00} | \hat{T}(\epsilon) | \mathbf{00} \rangle \simeq \tilde{W}^{+-}(\mathbf{0})$.

Now, let us consider the exciton-exciton interaction with anti-parallel spins. Since the exchange interaction does not exist at zero momentum, $\tilde{W}^{+-}(\mathbf{0}) \simeq 0$ takes place^{47,48}. Thus, within the first order Born approximation, excitons with anti-parallel spins do not interact. However, based on the result of Ref⁴³, now we will show

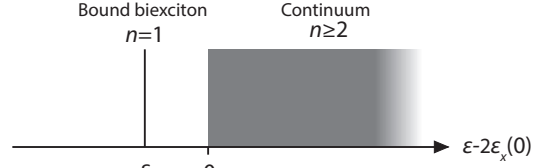


FIG. 10. The bound biexciton state and scattering continuum states.

that excitons with anti-parallel spins do interact due to the higher order contribution of the T-matrix. Firstly, let us examine the structure of the two-exciton states defined in Eq. 66. In general, the two-exciton states composed of molecular bound states and unbound continuum states (also referred to as unbound biexcitons)^{44,49,50}. The energy of the bound states is lower than that of two free excitons. On the other hand, the energy of the unbound continuum states is higher than the two free excitons and the number of unbound states is infinite. In the case of GaAs quantum well, it is known that the bare exciton-exciton interaction potential $\tilde{W}^{+-}(\mathbf{q})$ includes one molecular bound state, which is nothing but the biexciton state considered in the main text. In addition to the biexciton, several calculation and experiments proved that the bare exciton-exciton interaction contains unbound continuum states, which is called “scattering continuum”^{51,52}. Thus, we assume that the $n = 1$ state is the bound biexciton state and its energy $\Omega_{\mathbf{0}}^{(1)}$ is written as ϵ_B . Now the scattering amplitude Eq. 71 reads:

$$\langle \mathbf{00} | \hat{T}(\epsilon) | \mathbf{00} \rangle \simeq \frac{g_{bx}^{(1)}(\mathbf{0}, \mathbf{0}, \mathbf{0})}{\epsilon - \epsilon_B} + \sum_{n=2}^{\infty} \frac{g_{bx}^{(n)}(\mathbf{0}, \mathbf{0}, \mathbf{0})}{\epsilon - \Omega_{\mathbf{0}}^{(n)}}. \quad (72)$$

The structure of the eigenenergies of the T-matrix is schematically depicted in Fig. 10. This is the main result of this appendix. In the effective exciton-exciton interaction Hamiltonian, the first part corresponds to the biexciton state and exciton-bexciton coupling. Meanwhile, the second part is the contribution to the scattering amplitude from the exciton continuum. As Eq. 72 shows, the exciton continuum contribution depends on the energies of the incident excitons, however, the $\Omega_{\mathbf{0}}^{(n)}$ are larger than the two free exciton energies and the energy dependence is not very sensitive, which is supported by the detailed calculation of the T-matrix in⁴³. Therefore, it may be allowed to replace the exciton continuum contribution as a constant g^{+-} . In this appendix, we considered only the exciton-exciton interaction with anti-parallel spins. However, the same discussion can be applied to the exciton-exciton interaction with parallel spins $\tilde{W}^{++}(\mathbf{q})$ ⁵². Since the biexciton is not formed between excitons with parallel spins, the scattering amplitude is not very sensitive to the energy of two excitons and the scattering continuum works just as an offset to the the lowest order term $\tilde{W}^{++}(\mathbf{0})$. The most important consequence of the the scattering continuum is appearance of the imaginary part of the T matrix. The imaginary part of the T matrix

is equivalent to the energy dependent imaginary part of the interaction constant, which might be interpreted as an origin of the excitation induced dephasing (EID) of the lower-polaritons in the positive cavity detuning α'_1 .

APPENDIX C: EFFECTIVE HAMILTONIAN OF POLARITON-BIEXCITON COUPLING

In the main text, the effective interaction constant α_2 (Eq. 48) is indirectly obtained considering a pump-probe measurement. In this Appendix, we attempt to directly derive an effective Hamiltonian representing the polaritonic Feshbach resonance but does not include biexciton operators. For this purpose, we make use of a canonical transformation called Schrieffer-Wolff transformation⁵³⁻⁵⁶, which is originally introduced for Kondo physics but also has been applied to the derivation of the electron-phonon effective interaction Hamiltonian in superconductivity^{54,55,57}. In superconductivity, the electron-phonon interaction gives rise to an effective attractive interaction between electrons through a phonon retardation effect (Bardeen-Pines interaction^{57,58}). Actually, the polaritonic Feshbach resonance, where the polariton interaction is mediated by biexcitons, is analogous to the phonon mediated electron interaction.

We consider Hamiltonian representing lower-polaritons, biexcitons and the polariton-biexciton coupling in a momentum space $\hat{H} = \hat{H}_0 + \hat{H}_I$:

$$\hat{H}_0 = \sum_{\sigma} \sum_{\mathbf{k}} \varepsilon_{L,\mathbf{k}} \hat{p}_{\mathbf{k},\sigma}^{\dagger} \hat{p}_{\mathbf{k},\sigma} + \sum_{\mathbf{q}} \varepsilon_{B,\mathbf{q}} \hat{m}_{\mathbf{q}}^{\dagger} \hat{m}_{\mathbf{q}} \quad (73)$$

and

$$\hat{H}_I = \sum_{\mathbf{k}\mathbf{q}} g_L^{bx} \left[\hat{p}_{\mathbf{k},\uparrow} \hat{p}_{-\mathbf{k}+\mathbf{q},\downarrow} \hat{m}_{\mathbf{q}}^{\dagger} + \hat{m}_{\mathbf{q}} \hat{p}_{\mathbf{k},\uparrow}^{\dagger} \hat{p}_{-\mathbf{k}+\mathbf{q},\downarrow}^{\dagger} \right]. \quad (74)$$

The Hamiltonian \hat{H}_0 and \hat{H}_I are the momentum space representation of the Hamiltonian (Eq. 16 and Eq. 17). The annihilation operators of a lower-polariton $\hat{p}_{\mathbf{k},\sigma}$ and a biexciton $\hat{m}_{\mathbf{k}}$ are related to the field operators as

$$\hat{\psi}_{L,\sigma}(\mathbf{x}) = \sum_{\mathbf{k}} \frac{1}{\sqrt{S}} e^{i\mathbf{k}\cdot\mathbf{x}} \cdot \hat{p}_{\mathbf{k},\sigma}, \quad (75)$$

and

$$\hat{\psi}_B(\mathbf{x}) = \sum_{\mathbf{k}} \frac{1}{\sqrt{S}} e^{i\mathbf{k}\cdot\mathbf{x}} \cdot \hat{m}_{\mathbf{k}}. \quad (76)$$

The energies $\varepsilon_{L,\mathbf{k}}$ and $\varepsilon_{B,\mathbf{k}}$ is given by

$$\varepsilon_{L(B),\mathbf{k}} = \varepsilon_{L(B)} + \frac{\hbar^2 \mathbf{k}^2}{2m_{L(B)}} \quad (77)$$

Now, we consider a canonical transformation of the type:

$$\begin{aligned} \hat{H}' &= e^{-\hat{S}} \hat{H} e^{\hat{S}} \\ &= \hat{H} + [\hat{H}, \hat{S}] + \frac{1}{2!} [[\hat{H}, \hat{S}], \hat{S}] + \dots \end{aligned} \quad (78)$$

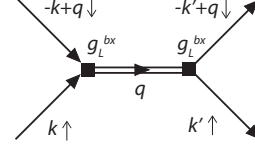


FIG. 11. Diagrammatic representation of the biexciton mediated effective polariton interaction, which is a second-order process. The arrow and the double line respectively represent a lower-polariton and a biexciton

When we chose the operator \hat{S} as to satisfy a relation:

$$[\hat{H}_0, \hat{S}] = -\hat{H}_I, \quad (79)$$

the the new Hamiltonian Eq. 78 leads to

$$\hat{H}' = e^{-\hat{S}} \hat{H} e^{\hat{S}} = \hat{H}_0 + \frac{1}{2} [\hat{H}_I, \hat{S}] + \dots \quad (80)$$

Here, we define an effective Hamiltonian \hat{H}_{eff} as

$$\hat{H}_{\text{eff}} \equiv \frac{1}{2} [\hat{H}_I, \hat{S}]. \quad (81)$$

In order to apply the canonical transformation to our Hamiltonian, we assume the operator \hat{S} of the form^{54,55}:

$$\hat{S} = \sum_{\mathbf{k}\mathbf{q}} g_L^{bx} \left[A_{\mathbf{k},\mathbf{q}} \hat{p}_{\mathbf{k},\uparrow} \hat{p}_{-\mathbf{k}+\mathbf{q},\downarrow} \hat{m}_{\mathbf{q}}^{\dagger} + B_{\mathbf{k},\mathbf{q}} \hat{m}_{\mathbf{q}} \hat{p}_{\mathbf{k},\uparrow}^{\dagger} \hat{p}_{-\mathbf{k}+\mathbf{q},\downarrow}^{\dagger} \right], \quad (82)$$

where the coefficient $A_{\mathbf{k},\mathbf{q}}$ and $B_{\mathbf{k},\mathbf{q}}$ are determined as to satisfy the condition Eq. 79. We find the quantity $[\hat{H}_0, \hat{S}]$ as

$$\begin{aligned} [\hat{H}_0, \hat{S}] &= \\ &= \sum_{\mathbf{k}\mathbf{q}} g_L^{bx} \left[A_{\mathbf{k},\mathbf{q}} (-\varepsilon_{L,\mathbf{k}} - \varepsilon_{L,-\mathbf{k}+\mathbf{q}} + \varepsilon_{B,\mathbf{q}}) \hat{p}_{\mathbf{k},\uparrow} \hat{p}_{-\mathbf{k}+\mathbf{q},\downarrow} \hat{m}_{\mathbf{q}}^{\dagger} \right. \\ &\quad \left. + B_{\mathbf{k},\mathbf{q}} (\varepsilon_{L,\mathbf{k}} + \varepsilon_{L,-\mathbf{k}+\mathbf{q}} - \varepsilon_{B,\mathbf{q}}) \hat{m}_{\mathbf{q}} \hat{p}_{\mathbf{k},\uparrow}^{\dagger} \hat{p}_{-\mathbf{k}+\mathbf{q},\downarrow}^{\dagger} \right]. \end{aligned} \quad (83)$$

In order to make this quantity equal to $-\hat{H}_I$, the coefficients $A_{\mathbf{k},\mathbf{q}}$ and $B_{\mathbf{k},\mathbf{q}}$ should be set as

$$A_{\mathbf{k},\mathbf{q}} = \frac{1}{\varepsilon_{L,\mathbf{k}} + \varepsilon_{L,-\mathbf{k}+\mathbf{q}} - \varepsilon_{B,\mathbf{q}}} = \frac{1}{\Delta_{\mathbf{k},\mathbf{q}}} \quad (84)$$

and

$$B_{\mathbf{k},\mathbf{q}} = \frac{1}{-\varepsilon_{L,\mathbf{k}} - \varepsilon_{L,-\mathbf{k}+\mathbf{q}} + \varepsilon_{B,\mathbf{q}}} = -\frac{1}{\Delta_{\mathbf{k},\mathbf{q}}}, \quad (85)$$

where $\Delta_{\mathbf{k},\mathbf{q}}$ is defined as

$$\Delta_{\mathbf{k},\mathbf{q}} = \varepsilon_{L,\mathbf{k}} + \varepsilon_{L,-\mathbf{k}+\mathbf{q}} - \varepsilon_{B,\mathbf{q}}. \quad (86)$$

Now, we find that the operator for the canonical transformation \hat{S} is given by

$$\hat{S} = \sum_{\mathbf{k}\mathbf{q}} g_L^{bx} \left[\frac{\hat{p}_{\mathbf{k},\uparrow} \hat{p}_{-\mathbf{k}+\mathbf{q},\downarrow} \hat{m}_{\mathbf{q}}^{\dagger}}{\Delta_{\mathbf{k},\mathbf{q}}} - \frac{\hat{m}_{\mathbf{q}} \hat{p}_{\mathbf{k},\uparrow}^{\dagger} \hat{p}_{-\mathbf{k}+\mathbf{q},\downarrow}^{\dagger}}{\Delta_{\mathbf{k},\mathbf{q}}} \right]. \quad (87)$$

Substituting this into Eq. 81, we obtain the effective Hamiltonian as

$$\begin{aligned}\hat{H}_{\text{eff}} &= \frac{1}{2}[\hat{H}_I, \hat{S}] \\ &= \frac{1}{2} \sum_{\mathbf{k}\mathbf{k}'\mathbf{q}} g_L^{bx^2} \left[\frac{1}{\Delta_{\mathbf{k}'\mathbf{q}}} + \frac{1}{\Delta_{\mathbf{k}\mathbf{q}}} \right] \\ &\quad \times \hat{p}_{\mathbf{k}'\uparrow}^\dagger \hat{p}_{-\mathbf{k}'+\mathbf{q}\downarrow}^\dagger \hat{p}_{-\mathbf{k}+\mathbf{q}\downarrow} \hat{p}_{\mathbf{k}\uparrow} + O(\hat{p}^\dagger \hat{p}),\end{aligned}\quad (88)$$

where the symbol $O(\hat{p}^\dagger \hat{p})$ represents terms that include only two lower-polariton operators \hat{p}^\dagger and \hat{p} . If we are interested only in low momentum interactions ($\mathbf{k} \sim \mathbf{k}' \sim \mathbf{q} \sim \mathbf{0}$), with an approximation:

$$\Delta_{\mathbf{k}\mathbf{q}} \simeq \Delta_{\mathbf{k}'\mathbf{q}} \simeq 2\varepsilon_L - \varepsilon_B, \quad (89)$$

the effective Hamiltonian is approximated as

$$\begin{aligned}\hat{H}_{\text{eff}} &\simeq \sum_{\mathbf{k}\mathbf{k}'\mathbf{q}} \left(\frac{g_L^{bx^2}}{2\varepsilon_L - \varepsilon_B} \right) \hat{p}_{\mathbf{k}'\uparrow}^\dagger \hat{p}_{-\mathbf{k}'+\mathbf{q}\downarrow}^\dagger \hat{p}_{-\mathbf{k}+\mathbf{q}\downarrow} \hat{p}_{\mathbf{k}\uparrow} \\ &= \left(\frac{g_L^{bx^2}}{2\varepsilon_L - \varepsilon_B} \right) \int d\mathbf{x} \hat{\psi}_{L,\uparrow}^\dagger \hat{\psi}_{L,\downarrow}^\dagger \hat{\psi}_{L,\downarrow} \hat{\psi}_{L,\uparrow}.\end{aligned}\quad (90)$$

The prefactor of this effective Hamiltonian is same as the resonance part of the coefficient α_2 (Eq. 48) with $\gamma_B = 0$. This effective Hamiltonian is equivalent to the second-order perturbation and the process is diagrammatically presented in Fig. 11. The diagram in Fig. 11 describes the biexciton mediated effective lower-polariton interaction. The polariton energy dependence of the effective Hamiltonian is due to the retardation effect of biexcitons. The advantage of the effective Hamiltonian is that since the Hamiltonian include only lower-polariton operators, we can eliminate the degree of freedom of biexciton.

* E-mail: naotomot@phys.ethz.ch

- ¹ C. Weisbuch, M. Nishioka, A. Ishikawa, and Y. Arakawa, *Phys. Rev. Lett.* **69**, 3314 (1992).
- ² J. Kasprzak, M. Richard, S. Kundermann, A. Baas, P. Jeambrun, J. M. J. Keeling, F. M. Marchetti, M. H. Szymanska, R. André, J. L. Staehli, V. Savona, P. B. Littlewood, B. Deveaud, and L. S. Dang, *Nature* **443**, 409 (2006).
- ³ A. Amo, J. Lefrère, S. Pigeon, C. Adrados, C. Ciuti, I. Carusotto, R. Houdré, E. Giacobino, and A. Bramati, *Nature Phys.* **5**, 805 (2009).
- ⁴ S. Utsunomiya, L. Tian, G. Roumpos, C. W. Lai, N. Kumada, T. Fujisawa, M. Kuwata-Gonokami, A. Löffler, S. Höfling, A. Forchel, and Y. Yamamoto, *Nature Phys.* **4**, 700 (2008).
- ⁵ V. Kohnle, Y. Léger, M. Wouters, M. Richard, M. T. Portella-Oberli, and B. Deveaud-Plédran, *Phys. Rev. Lett.* **106**, 255302 (2011).
- ⁶ V. Kohnle, Y. Léger, M. Wouters, M. Richard, M. T. Portella-Oberli, and B. Deveaud, *Phys. Rev. B* **86**, 064508 (2012).
- ⁷ P. Borri, W. Langbein, U. Woggon, J. R. Jensen, and J. M. Hvam, *Phys. Rev. B* **62**, R7763 (2000).
- ⁸ S. Inouye, M. R. Andrews, J. Stenger, H.-J. Miesner, D. M. Stamper-Kurn, and W. Ketterle, *Nature* **392**, 151 (1998).
- ⁹ M. Wouters, *Phys. Rev. B* **76**, 045319 (2007).
- ¹⁰ I. Carusotto, T. Volz, and A. Imamoglu, *EPL (Europhysics Letters)* **90**, 37001 (2010).
- ¹¹ M. Vladimirova, S. Cronenberger, D. Scalbert, K. V. Kavokin, A. Miard, A. Lemaître, J. Bloch, D. Solnyshkov, G. Malpuech, and A. V. Kavokin, *Phys. Rev. B* **82**, 075301 (2010).
- ¹² N. Takemura, S. Trebaol, M. Wouters, M. T. Portella-Oberli, and B. Deveaud, *Nature Physics* **10**, 500 (2014).
- ¹³ B. L. Wilmer, F. Passmann, M. Gehl, G. Khitrova, and A. D. Bristow, *Phys. Rev. B* **91**, 201304 (2015).
- ¹⁴ H. Oka and H. Ishihara, *Phys. Rev. Lett.* **100**, 170505 (2008).
- ¹⁵ F. M. Marchetti and J. Keeling, *Phys. Rev. Lett.* **113**, 216405 (2014).
- ¹⁶ W. Casteels and M. Wouters, *Phys. Rev. A* **90**, 043602 (2014).
- ¹⁷ I. A. Shelykh, A. V. Kavokin, Y. G. Rubo, T. C. H. Liew, and G. Malpuech, *Semiconductor Science and Technology* **25**, 013001 (2010).
- ¹⁸ N. Takemura, S. Trebaol, M. Wouters, M. T. Portella-Oberli, and B. Deveaud, *Phys. Rev. B* **90**, 195307 (2014).
- ¹⁹ N. Takemura, M. D. Anderson, S. Biswas, M. Navadeh-Toupchi, D. Y. Oberli, M. T. Portella-Oberli, and B. Deveaud, *Phys. Rev. B* **94**, 195301 (2016).
- ²⁰ R. P. Stanley, R. Houdr, U. Oesterle, M. Gailhanou, and M. Ilegems, *Appl. Phys. Lett.* **65**, 1883 (1994).
- ²¹ G. Rochat, C. Ciuti, V. Savona, C. Piermarocchi, A. Quattropani, and P. Schwendimann, *Phys. Rev. B* **61**, 13856 (2000).
- ²² M. Kuwata-Gonokami, T. Aoki, C. Ramkumar, R. Shimano, and Y. P. Svirko, *Journal of Luminescence* **8789**, 162 (2000).
- ²³ N. P. Proukakis, K. Burnett, and H. T. C. Stoof, *Phys. Rev. A* **57**, 1230 (1998).
- ²⁴ M. Combescot, M. A. Dupertuis, and O. Betbeder-Matibet, *EPL (Europhysics Letters)* **79**, 17001 (2007).
- ²⁵ C. Ciuti, P. Schwendimann, B. Deveaud, and A. Quattropani, *Phys. Rev. B* **62**, R4825 (2000).
- ²⁶ E. Timmermans, P. Tommasini, R. Côté, M. Hussein, and A. Kerman, *Phys. Rev. Lett.* **83**, 2691 (1999).
- ²⁷ E. Timmermans, P. Tommasini, M. Hussein, and A. Kerman, *Physics Reports* **315**, 199 (1999).
- ²⁸ M. Mackie, K.-A. Suominen, and J. Javanainen, *Phys. Rev. Lett.* **89**, 180403 (2002).
- ²⁹ I. Carusotto and C. Ciuti, *Phys. Rev. Lett.* **93**, 166401 (2004).
- ³⁰ L. Pitaevskii and S. Stringari, "Bose-einstein condensation (international series of monographs on physics)," (2003).
- ³¹ E. M. Lifshitz and L. P. Pitaevskii, *Statistical physics, vol. 2* (Pergamon, Oxford, 1980).
- ³² A. L. Fetter and J. D. Walecka, *Quantum theory of many-particle systems* (Courier Corporation, 2003).

- ³³ M. Wouters and I. Carusotto, Phys. Rev. B **79**, 125311 (2009).
- ³⁴ J. M. Zajac and W. Langbein, Phys. Rev. B **92**, 165305 (2015).
- ³⁵ M. Theis, G. Thalhammer, K. Winkler, M. Hellwig, G. Ruff, R. Grimm, and J. H. Denschlag, Phys. Rev. Lett. **93**, 123001 (2004).
- ³⁶ N. Takemura, M. D. Anderson, S. Trebaol, S. Biswas, D. Y. Oberli, M. T. Portella-Oberli, and B. Deveaud, Phys. Rev. B **92**, 235305 (2015).
- ³⁷ A. Amo, T. C. H. Liew, C. Adrados, R. Houdré, E. Giacobino, A. V. Kavokin, and A. Bramati, Nature Phot. **4**, 361 (2010).
- ³⁸ D. Sarkar, S. S. Gavrilov, M. Sich, J. H. Quilter, R. A. Bradley, N. A. Gippius, K. Guda, V. D. Kulakovskii, M. S. Skolnick, and D. N. Krizhanovskii, Phys. Rev. Lett. **105**, 216402 (2010).
- ³⁹ M. Wouters, T. K. Paraiso, Y. Léger, R. Cerna, F. Morier-Genoud, M. T. Portella-Oberli, and B. Deveaud-Plédran, Phys. Rev. B **87**, 045303 (2013).
- ⁴⁰ M. Saba, F. Quochi, C. Ciuti, U. Oesterle, J. L. Staehli, B. Deveaud, G. Bongiovanni, and A. Mura, Phys. Rev. Lett. **85**, 385 (2000).
- ⁴¹ U. Neukirch, S. R. Bolton, N. A. Fromer, L. J. Sham, and D. S. Chemla, Phys. Rev. Lett. **84**, 2215 (2000).
- ⁴² C. J. Pethick and H. Smith, *Bose-Einstein condensation in dilute gases* (Cambridge university press, 2002).
- ⁴³ R. Takayama, N. H. Kwong, I. Rumyantsev, M. Kuwata-Gonokami, and R. Binder, The Eur. Phys. Jour. B **25**, 445 (2002).
- ⁴⁴ L. S. Rodberg and R. M. Thaler, *Introduction to the quantum theory of scattering* (Academic Press, 1967).
- ⁴⁵ A. L. Ivanov, M. Hasuo, N. Nagasawa, and H. Haug, Phys. Rev. B **52**, 11017 (1995).
- ⁴⁶ N. H. Kwong, R. Takayama, I. Rumyantsev, M. Kuwata-Gonokami, and R. Binder, Phys. Rev. B **64**, 045316 (2001).
- ⁴⁷ C. Ciuti, V. Savona, C. Piermarocchi, A. Quattropani, and P. Schwendimann, Phys. Rev. B **58**, 7926 (1998).
- ⁴⁸ J.-i. Inoue, T. Brandes, and A. Shimizu, Phys. Rev. B **61**, 2863 (2000).
- ⁴⁹ M. Combescot and R. Combescot, Phys. Rev. Lett. **61**, 117 (1988).
- ⁵⁰ H. Oka and H. Ishihara, Phys. Rev. B **78**, 195314 (2008).
- ⁵¹ V. M. Axt, K. Victor, and T. Kuhn, physica status solidi (b) **206**, 189 (1998).
- ⁵² N. H. Kwong, R. Takayama, I. Rumyantsev, M. Kuwata-Gonokami, and R. Binder, Phys. Rev. Lett. **87**, 027402 (2001).
- ⁵³ J. R. Schrieffer and P. A. Wolff, Phys. Rev. **149**, 491 (1966).
- ⁵⁴ P. L. Taylor and O. Heinonen, *A quantum approach to condensed matter physics* (Cambridge University Press, 2002).
- ⁵⁵ P. Phillips, *Advanced solid state physics* (Cambridge University Press, 2012).
- ⁵⁶ C. Cohen-Tannoudji, J. Dupont-Roc, G. Grynberg, and P. Thickstun, *Atom-photon interactions: basic processes and applications* (Wiley Online Library, 1992).
- ⁵⁷ H. Fröhlich, Proceedings of the Royal Society of London A: Mathematical, Physical and Engineering Sciences **215**, 291 (1952).
- ⁵⁸ J. Bardeen and D. Pines, Phys. Rev. **99**, 1140 (1955).